In silico design of novel and highly selective lysine-specific histone demethylase inhibitors

Ebru Demet AKDOĞAN[1]**, Burak ERMAN**[2]**, Kemal YELEKÇİ**[1,*]

[1]*Department of Information Technologies, Kadir Has University, Cibali,*
34083 İstanbul-TURKEY
e-mail: yelekci@khas.edu.tr
[2]*Department of Chemical and Biological Engineering, Koç University,*
34450 İstanbul-TURKEY

Histone lysine-specific demethylase (LSD1) is involved in a wide range of epigenetic processes and plays important roles in gene silencing, DNA transcription, DNA replication, DNA repair, and heterochromatin formation. Its active site shows a resemblance to those of 2 homologous enzymes, monamine oxidase A and B (MAO-A and MAO-B.) In the present work, starting from suitable scaffolds and generating thousands of structures from them, 10 potential inhibitors were obtained with structural and physicochemical properties selectively suitable for inhibiting LSD1. iLib Diverse software was used to generate the diverse structures and 3 docking tools, CDOCKER, GOLD, and AutoDock, were used to find the most probable potential inhibitor based on its binding affinity. The dispositions of the candidate molecules within the organism were checked by ADMET_PSA_2D (polar surface area) versus ADMET_AlogP98 (the logarithm of the partition coefficient between n-octanol and water), and their suitability is discussed. The LSD1 inhibition activities of the candidates were compared with the properties of trans-2-phenylcyclopropylamine (tranylcypromine) and 2-(4-methoxy-phenyl) cyclopropylamine, which are the 2 known inhibitors of LSD1.

Key Words: LSD1, monamine oxidase, de novo design, selective inhibitors

Introduction

The first human histone lysine-specific demethylase (LSD1) discovered in 2004 specifically catalyzes the demethylation of mono- and dimethylated Lys_4 of histone H3 (H3K4) at the N-terminal.[1] Lysine methylation/demethylation

---

*Corresponding author

has recently attracted much attention owing to its involvement in a wide range of epigenetic processes that regulate cell fate and identity. LSD1 is shown to play important roles in gene silencing, as well as DNA transcription, replication, and repair and heterochromatin formation.

LSD1 (alias BHC110) is a flavin adenine dinucleotide (FAD)-dependent enzyme that catalyzes the oxidative removal of 1 or 2 methyl groups from H3K4, releasing formaldehyde and hydrogen peroxide.[1,2] LSD1 takes part in a transcriptional repressor complex, with the repressor protein CoREST and HDAC1 or HDAC2, leading to gene silencing.[3] LSD1 has been found to be upregulated in certain high-risk tumors[4,5] and thus the development of LSD1 inhibitors may represent a significant weapon against cancer.

To date, only 2 drugs, tranylcypromine[6,7] and 2-[4-methoxy-phenyl]cyclopropylamine,[1,2] have been described as LSD1 inhibitors, yet their action is not specific (they are well-known anti-MAO agents), and no experimental data are available about their effects on cancer diseases. Pargyline blocks demethylation by LSD1, and consequently it prevents androgen receptor-dependent transcription. Thus, modulation of LSD1 activity offers a new strategy to regulate androgen receptor functions, which may turn out to be crucial in prostate cancer models[2]

Biguanide and bisguanidine polyamine analogs have been said to affect a reexpression of multiple, aberrantly silenced genes important in the development of colon cancer, including members of the secreted frizzle-related proteins (SFRPs) and the GATA family of transcription factors.[7]

As a second kind of histone lysine demethylase, the jumonji-containing demethylases (such as JHDM1, JMJD2, and JMJD3) use ferrous iron (II) and 2-oxoglutarate (2OG) as cofactors to mediate a hydroxylation-based demethylation, and can only be Kme1, Kme2, or Kme3 demethylases (JHDM1, JMJD2, and JMJD3, respectively).[8−10] Some members of the JMJD2 family have been implicated in tumorigenesis, and JMJD3 has been found to be upregulated in prostate cancer.[11] Recently, Rose et al. discovered N-oxalyl-D-tyrosine derivatives as potent and selective inhibitors of JMJD2E.[12] They also obtained the crystal structure of JMJD2A in complex with one of the potent inhibitors. Therefore, the discovery of JmjC (jumonji domain C) [13]-containing enzyme inhibitors may be very useful in cancer therapy.

The development of a new generation of inhibitors for LSD1 has attracted the attention of many researchers working in design, synthesis, and molecular modeling studies. The similarity of LSD1 to other FAD-dependent enzymes such as MAO-A and MAO-B[14,15] presents an additional difficulty in finding a selective inhibitor for LSD1. Design of reversible and selective inhibitors for LSD1 requires special care and extra effort.

The elucidation of the 3D structure of LSD1 by X-ray crystallography opened the way for molecular modeling and in silico studies.[16] The structure of LSD1 includes 3 major domains, a C-terminal amine oxidase-like (AOL) domain homologous to FAD-dependent oxidases,[17−19] an N-terminal SWIRM domain, and the Tower domain. The AOL domain includes 2 subdomains, a FAD-binding and a substrate-binding domain that form a large cavity at the interface, which serves as the catalytic site. Here, lysine 661 (K661) is a crucial residue, which is hydrogen-bonded to the N5 atom of the FAD molecule. At the entrance of the cavity, there is an additional binding site, which is highly acidic. In vitro enzymatic assays by Forneris et al.[20] showed that LSD1 requires the first 20 N-terminal amino acids of the histone tail for productive binding.

In this study, by employing various molecular recognition techniques, several thousands of possible drug candidates were screened in silico and 10 potential LSD1 inhibitors are presented. This is the first computational work on LSD1 that explains the binding site with potential novel inhibitors and interacting residues.

Materials and methods

Crystal structure of LSD1

The crystal structures of LSD1, MAO-A, and MAO-B were extracted from the Protein Data Bank (PDB) (http://www.rcsb.org). Their PDB codes are 2DW4, 2Z5X, and 1OJA, respectively. Each structure was cleaned of all water molecules and inhibitors as well as all noninteracting ions before being used in the docking studies. In case the inhibitor was covalently bound to the FAD, the initial oxidized form of the FAD was used. For MAO-A and MAO-B, 1 of the 2 subunits was taken as the target structure. Using a fast Dreiding-like force field, each protein's geometry was first optimized and then submitted to the "Clean Geometry" toolkit of Discovery Studio (Accelerys, Inc.) for a more complete check. Missing hydrogen atoms were added based on the protonation state of the titratable residues at a pH of 7.4. Ionic strength was set to 0.145 and the dielectric constant was set to 10.

Generation of potential inhibitors

The design approach was based on the structure of the active site cavities of LSD1, MAO-A, and MAO-B. A few scaffolds were created and used for the derivation of leads and scaffolds using the commercial software iLib Diverse program.[21] Trans-2-phenyl cyclopropylamine (tranylcypromine) and 2-(4-methoxy-phenyl)cyclopropylamine compounds were also taken from the literature in order to compare their reported experimental and computational binding energy and inhibition constant values to the ones that were obtained in our study. In some inhibitors, 5-methyl-2-benzoxazolidinone scaffolds were used to generate selective LSD1 inhibitors. The others were individually selected from various leads. Table 1 lists all 10 potential inhibitors with their structural and their physicochemical properties.

Docking tools

Three popular software tools, CDOCKER,[22] GOLD,[23] and AutoDock,[24] were used to find the most probable potential inhibitor based on its binding affinity. CDOCKER uses a molecular dynamics-based algorithm while GOLD and AutoDock both use a genetic algorithm for the conformational search. The details of the software packages are given below.

CDOCKER

CDOCKER (<u>C</u>HARMm-based <u>DOCKER</u>) by Discovery Studio-2.5.5 uses the CHARMm family of force fields[25] and a grid-based molecular dynamics (MD) docking algorithm, and offers all the advantages of full ligand flexibility (including bonds, angles, and dihedrals) and reasonable computation times. Basically, it involves the generation of several random ligand conformations inside the active site of the target protein, followed by MD-based simulated annealing, which is composed of several heating and cooling stages, and final refinement by energy minimization. CDOCKER uses soft-core potentials, which are found to be effective in exploring the conformational space of small organics and macromolecules and are used in various docking studies.[26−28] The nonbonded interactions that include van der Waals (vdW) and electrostatics are softened at different levels, except during the final minimization step.

Table 1. List of 10 potential inhibitor molecules and 2 test compounds with their structural and physicochemical properties.
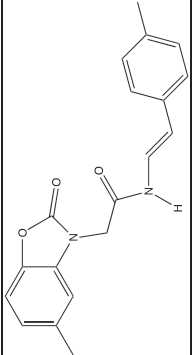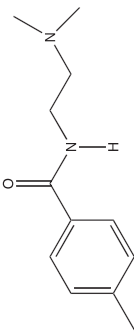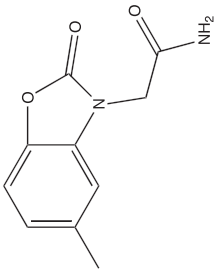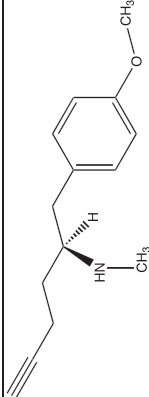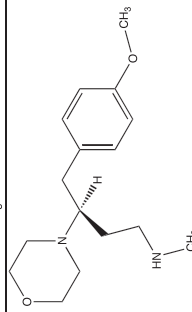
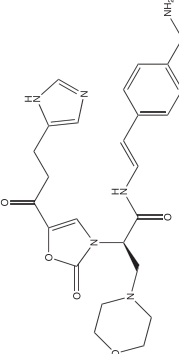| Compound Number	Chemical Formula	Chemical sketches	MW (g/mol)	Number of rotatable bonds	Number of HD[1]	Number of HA[2]	AlogP
1	$C_{19}H_{19}N_2O_3$		322.358	4	1	3	3.097
2	$C_{12}H_{18}N_2O$		206.248	4	1	2	1.663
3	$C_{10}H_{10}N_2O_3$		206.197	2	1	3	0.886
4	$C_{15}H_{21}NO$		231.333	7	1	2	4.001
5	$C_{16}H_{26}N_2O_2$		278.389	7	1	4	1.59

Table 1. Continued.
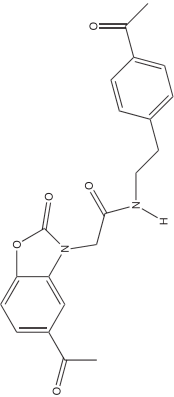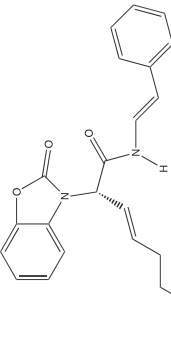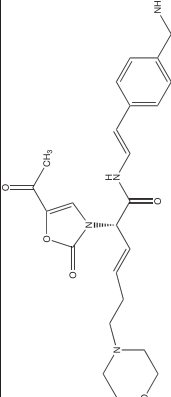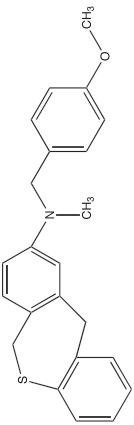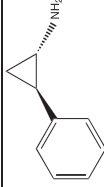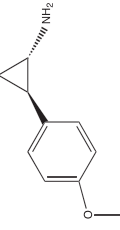
Compound Number	Chemical Formula	Chemical sketches	MW (g/mol)	Number of rotatable bonds	Number of HD[1]	Number of HA[2]	AlogP
6	$C_{20}H_{20}N_2O_2$		368.383	7	1	5	2.234
7	$C_{27}H_{29}N_3O_5$		475.586	9	1	6	2.615
8	$C_{24}H_{30}N_4O_5$		454.518	10	2	7	-0.161
9	$C_{25}H_{30}N_6O_5$		494.542	11	3	8	-1.037

Table 1. Continued.

Compound Number	Chemical Formula	Chemical sketches	MW (g/mol)	Number of rotatable bonds	Number of HD[1]	Number of HA[2]	AlogP
10	$C_{29}H_{31}NOS$		441.627	8	0	3	8.479
11	$C_{9}H_{11}N$		133.190	1	1	1	1.193
12	$C_{10}H_{13}NO$		163.216	2	1	2	1.177

[1] Number of hydrogen bond donor groups
[2] Number of hydrogen bond acceptor groups

Initially, 10 replicas[29] for each inhibitor are generated in the active site of the target protein, which is created as a spherical region with a diameter of 12 Å and centered on the FAD molecule. Simulated annealing is performed using a flexible ligand and a rigid protein. The ligand-protein interactions are computed from grid extension 8.0. Random conformations are generated using 1000 MD steps, while the system is heated to 1000 K in 2000 steps. In the simulated annealing stage, the number of heating steps is set to 2000, the heating target temperature to 700 K, cooling steps to 5000, and the cooling target temperature to 300 K.

The final refinement step of minimization is performed with full potential. Final minimized docking poses are then clustered, based on a heavy atom RMSD approach using a tolerance of 0.5 Å.[30] The final ranking is based on the total docking energy, which is composed of the ligand's intramolecular energy and the ligand-protein interaction. The Discovery Studio-2.5.5 visualization tool is used to analyze the 10 top hit conformations.

GOLD

The commercial software GOLD v.4.011 (Genetic Optimization for Ligand Docking) with GoldScore and ChemScore fitness functions was utilized.[23] The GoldScore fitness function, which is utilized to predict peptide binding positions, is based on H-bonding, van der Waals energies, and ligand torsion strain terms. The ChemScore fitness function is utilized to predict the total free energy change upon peptide binding to the predetermined binding site. The docking is executed by the genetic algorithm procedure of the GOLD program. The binding site is selected as a spherical region with a diameter of 10 Å and centered on the FAD molecule; 10 solutions are generated for each molecule and the best solution is further analyzed.

AutoDock

AutoDock uses a semiempirical force field based on the AMBER force field.[31−33] It uses a molecular mechanics model for enthalpic contributions such as vdW and hydrogen bonding, and an empirical model for entropic changes upon binding. Each component is multiplied by empirical weights obtained from the calibration against a set of known binding constants. AutoDock uses a Lamarckian genetic algorithm for the conformational search.[24] For each molecule, 50 independent runs are performed. A total of 300 distinct ligand conformers are initially generated and positioned randomly in the binding pocket. They have randomly assigned torsion angles to rotatable bonds and a randomly assigned overall rotation. A maximum of 100 million energy evaluations are allowed for each docking. A precalculated 3-dimensional energy grid of equally spaced discrete points is generated prior to docking, for a rapid energy evaluation, using the program AutoGrid.[34] The grid box, with dimensions of 30 × 30 × 30 Å, is centered at the N5 atom of the FAD molecule and covers the entire binding site and its neighboring residues. The distance between 2 grid points is set to 0.375 Å.

The best poses obtained from GOLD for each compound are further evaluated via HyperChem energy calculations, which are performed in a vacuum, using the BioCHARMm molecular mechanics force field with scale factors of 0.5 for the electrostatic and 0.125 for the van der Waals interactions. The reported values in Table 2 were obtained as the difference between the energy of the bound complex and the energy of the ligand alone. Energy minimization was performed using the steepest descent algorithm with a termination condition of an RMS gradient of 0.1 kcal/(Å-mol).

Table 2. Highest CDOCKER, GOLD, and AutoDock scores of 10 potential LSD inhibitors and 2 test compounds. The results that failed to bind are labeled as F.

Compound Number	LSD1					MAO-A					MAO-B				
	- CDocker Score	Gold Score	AutoDock Score	Chem Score	Hyper Chem	- CDocker Score	Gold Score	AutoDock Score	Chem Score	Hyper Chem	- CDocker Score	Gold Score	AutoDock Score	Chem Score	Hyper Chem
1	11.44	10.34	8.49	7.08	35.0	4.28	16.57	9.80	8.92	18.1	F	-170.7	6.27	9.77	F
2	21.65	19.17	6.38	6.43	28.5	13.95	21.03	6.01	6.19	34.7	-61.58	-76.63	5.91	8.13	F
3	1.97	24.89	5.83	4.64	25	8.63	30.49	7.06	5.33	22.2	-47.62	-38.3	6.22	5.23	F
4	24.20	19.22	6.73	6.92	17.9	-7.88	35.33	7.56	7.27	28.0	-113.17	-111.68	6.43	9.15	F
5	21.28	6.07	7.58	6.98	38.5	-67.00	11.48	6.96	6.88	25.2	-248.92	-205.16	6.08	9.90	F
6	16.78	22.88	8.47	6.13	38.1	8.04	19.48	10.45	8.06	F	F	-83.86	5.91	9.76	F
7	2.69	-9.00	9.78	8.28	43.6	F	-46.42	9.98	11.23	F	F	-434.1	6.16	14.19	F
8	8.73	33.67	9.38	7.15	53.9	-261.32	0.89	9.64	9.91	F	F	-216.90	5.40	12.57	F
9	27.88	35.69	8.52	6.39	58.8	F	3.03	9.38	9.52	F	F	4.19	5.88	9.57	F
10	27.28	1.00	9.86	10.79	36.5	F	-31.65	11.10	13.45	F	F	-470.58	6.09	17.46	F
11	10.85	5.14	5.81	2.91	10.0	10.51	16.34	5.57	3.11	2.6	14.10	10.99	6.17	3.30	9.0
12	9.25	17.25	6.15	5.35	19.8	13.15	25.32	5.49	6.53	23.0	-25.52	5.03	5.79	5.92	F

[1] Number of hydrogen bond donor groups
[2] Number of hydrogen bond acceptor groups

Results and discussion

Starting from various scaffolds and leading structures, a few thousand compounds were derived based on the structure of the LSD1 enzyme. Then, using 5 different scoring functions, these compounds were docked against LSD1, MAO-A, and MAO-B enzymes, all 3 of which have the same FAD cofactor. The 10 compounds with the highest scores and LSD1 selectivity were chosen and are listed in Table 2. The score values of 2 test compounds, tranylcypromine and 2-(4-methoxy-phenyl)cyclopropylamine, which are well-known inhibitors of LSD1, MAO-A, and MAO-B, were also listed for comparison (compounds **11** and **12**). Figure 1 illustrates the score values, with vertical bars for a visual comparison. In all 3 graphs (Figures 1a-1c), the bars on the negative side indicate that the compound either failed to dock to the enzyme or was bound very poorly. It is clear that the AutoDock and ChemScore score values were all positive and close to each other in all 3 enzymes and therefore those systems cannot identify the selectivity of LSD1 as strongly as HyperChem, GOLD, and CDOCKER, which all showed failed or poor binding of most compounds to MAO-A and MAO-B.
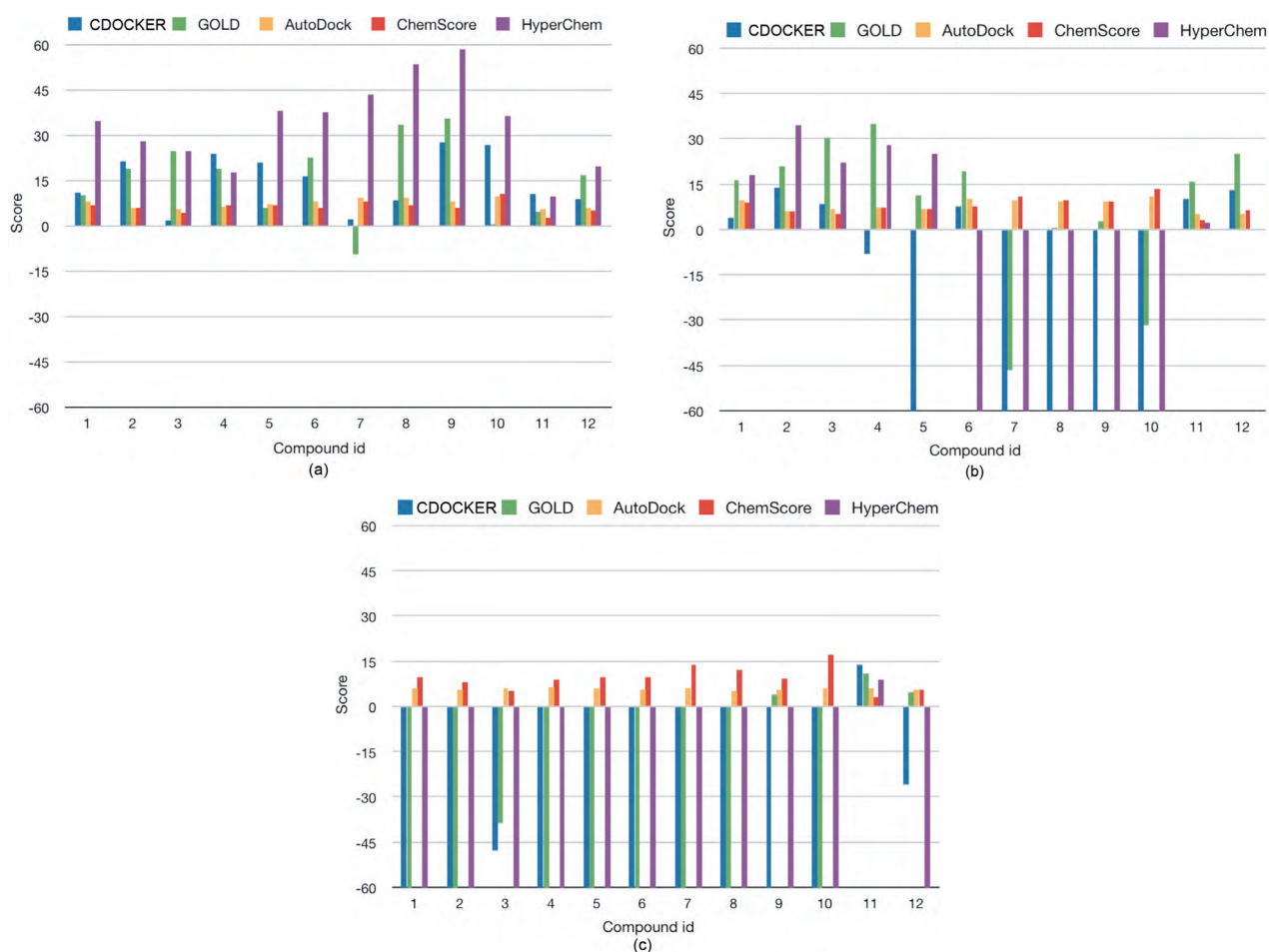

Figure 1. The 5 different score values for the best pose of the potential drug candidate for a) LSD1, b) MAO-A, and c) MAO-B. The compound ID is given as in Table 2.

Table 3 gives a selectivity report for all 10 compounds. The sign $\sqrt{}$ indicates that the drug candidate had the highest affinity for LSD1 rather than MAO-A or MAO-B. More than half of the compounds showed LSD1 selectivity, which was confirmed by at least 2 docking programs. In general, the MAO-A activity was found to be superior to that of MAO-B activity in all 10 compounds. Most of the designed compounds either failed to dock into the MAO-B enzyme active site or were bound to the enzyme very poorly.

Table 3. Selectivity report. The sign $\sqrt{}$ indicates that the drug candidate has the highest affinity for LSD1 rather than MAO-A or MAO-B.

Compound Number	CDOCKER	GOLD	AutoDock	ChemScore	HyperChem
1	$\sqrt{}$				$\sqrt{}$
2	$\sqrt{}$		$\sqrt{}$	$\sqrt{}$	
3					$\sqrt{}$
4	$\sqrt{}$				
5	$\sqrt{}$		$\sqrt{}$	$\sqrt{}$	$\sqrt{}$
6	$\sqrt{}$	$\sqrt{}$			$\sqrt{}$
7	$\sqrt{}$	$\sqrt{}$			$\sqrt{}$
8	$\sqrt{}$	$\sqrt{}$			$\sqrt{}$
9	$\sqrt{}$	$\sqrt{}$			$\sqrt{}$
10	$\sqrt{}$	$\sqrt{}$			$\sqrt{}$

Figure 2 shows the ADMET_PSA_2D (polar surface area) versus the ADMET_AlogP98 (the logarithm of the partition coefficient between n-octanol and water). The ellipses define the regions where well-absorbed inhibitors are expected to be located. For intestinal absorption, 95% and 99% of well-absorbed inhibitors are expected to fall within the ellipses colored in red and green, respectively. Similarly, for overcoming the blood-brain barrier, 95% and 99% of well-absorbed inhibitors are expected to fall within the ellipses colored with magenta and aqua, respectively. All 7 compounds were found inside all 4 ellipses, therefore satisfying the conditions for absorption by the intestines and the brain. Compound **8** satisfies only the condition for overcoming the blood-brain barrier. Compounds **9** and **10** are found outside all ellipses.

In Table 4, CDOCKER and AutoDock scores of tranylcypromine enantiomers are listed with their experimental inhibition constants.[16,35,36] Both compounds showed a higher affinity for MAO-B than LSD1. Despite the fact that experimental results were reported for the covalent inhibition of (+)-tPCPA and (-)-tPCPA enantiomers, their noncovalent binding affinities predicted via AutoDock and CDOCKER agree well with experimental findings. For MAO-A, there are no experimental results reported; however, our in silico calculations indicate that the affinity of the 2 enantiomers for MAO-A is the lowest among the 3 enzymes.

As seen from Table 3, the highest LSD1 selectivity was obtained for compounds **2** and **5**. Compound **2** holds the highest score for LSD1 in 3 different scoring functions, while compound **5** holds the highest score in 4 different scoring functions. Hence, they were selected for further discussion in detail, via 2- and 3-dimensional illustrations produced by Accelerys visualization tools. Figures 3-8 show the best-docked conformation of compound **2** in LSD1, MAO-A, and MAO-B enzymes obtained from the CDOCKER program. Docking energies of the best pose of compound **2** against LSD1, MAO-A, and MAO-B were determined as –21.65, –13.95, and
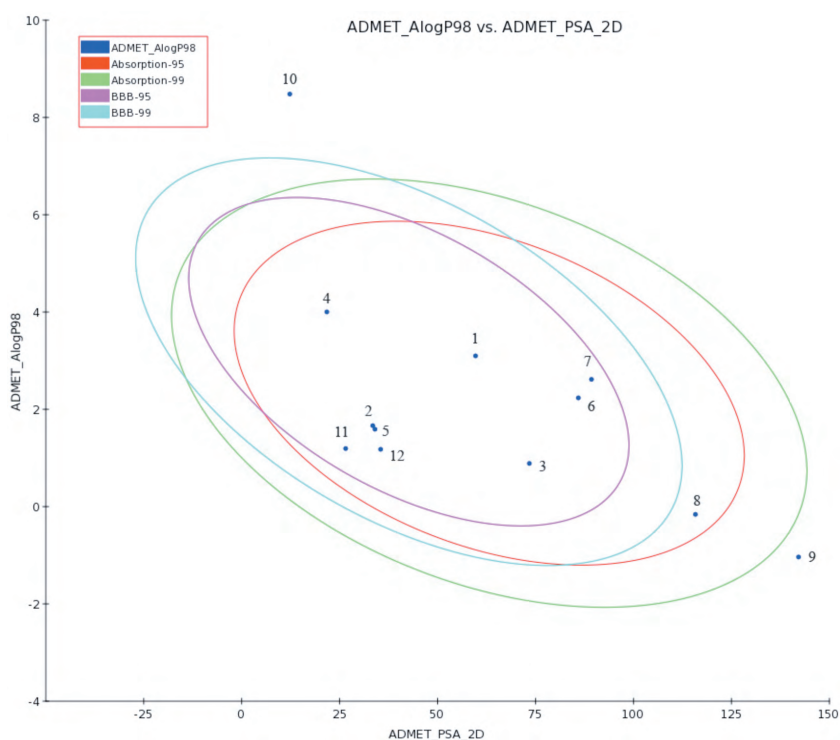
Figure 2. ADMET plot. ADMET_PSA_2D (polar surface area) versus ADMET_AlogP98 (the logarithm of the partition coefficient between n-octanol and water).
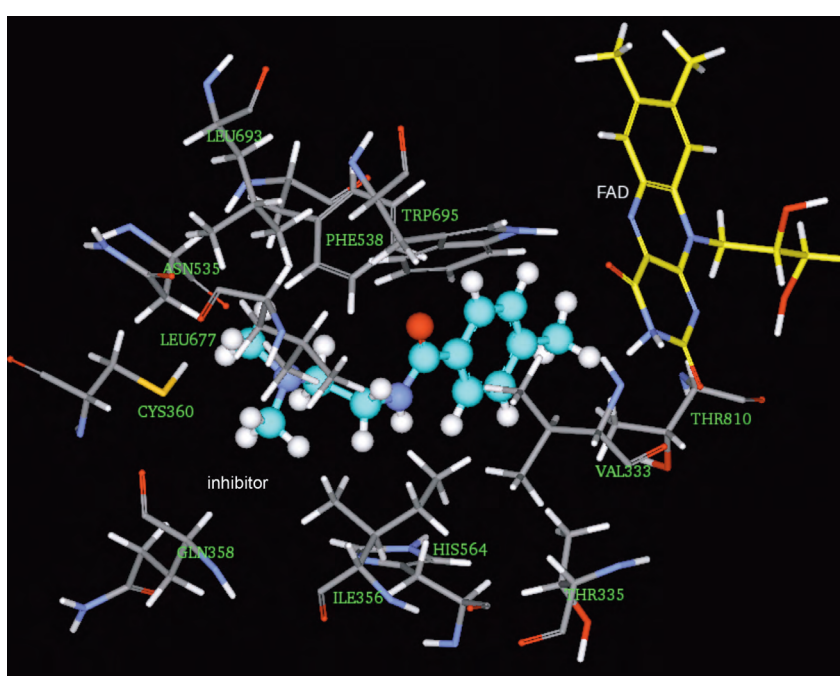

Figure 3. The 3-dimensional orientation of compound **2** in the active site of the LSD1 enzyme. Amino acid side chains are shown as sticks, the inhibitor is shown as a ball and stick, and the cofactor FAD is depicted as a yellow stick.

+61.58 kcal/mol, respectively. A more negative value indicates more favorable binding. In Figure 4, a 2-dimensional interaction diagram of the best pose with its surrounding residues is illustrated. Here, residues colored in green are involved in vdW interactions, whereas those in magenta make hydrogen bonds or electrostatic interactions with the inhibitor. The inhibitor is surrounded closely in the active site by 15 vdW interactions. Additionally, there is one $\pi - \pi$ interaction between the FAD and the 4-methyl phenyl group of the inhibitor and one polar attraction between the CYS360 side chain and the inhibitor.

Table 4. Highest CDOCKER and AutoDock scores and experimental free energy of binding of (+) and (-) enantiomers of tranylcypromine.

Compounds	LSD1			MAO-A			MAO-B		
	Exp (μM)	AutoDock (μM)	CDOCKER (kcal/mol)	Exp (μM)	AutoDock (μM)	CDOCKER	Exp (μM)	AutoDock (μM)	CDocker (kcal/mol)
(+)-tPCPA	284	40.27	−11.62	NA*	81.78	−10.56	4.4	29.72	−14.30
(-)-tPCPA	168	53.59	−10.85	NA	89.33	−10.51	89	29.95	−14.10

*Undetermined

The best poses of compound **2** in the active site of MAO-A are shown in Figures 5 and 6. Here, the number of vdW interactions is decreased to 11. In addition, the GLN215, PHE208, and CYS323 side chains interact with compound **2** via hydrogen bonds and electrostatics. However, the distances between the interacting side chains and compound **2** are not as close as in LSD1. The CDOCKER energy of this compound was −13.95 kcal/mol, which is nearly half of its value in the LSD1 enzyme, which was −21.65 kcal/mol.
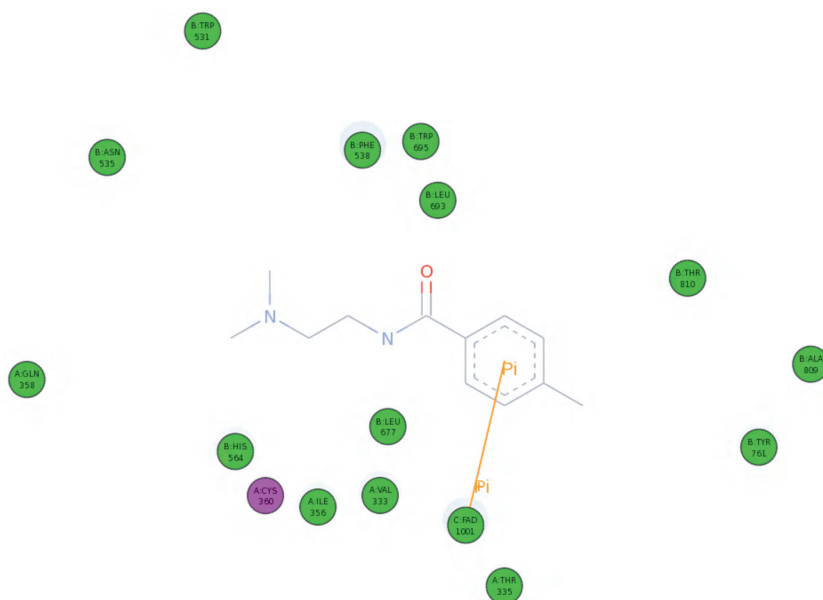

Figure 4. The 2-dimensional picture of compound **2** in the active site of the LSD1 enzyme. Residues involved in hydrogen bonding or polar interactions are represented by magenta-colored circles, and residues involved in vdW and hydrophobic interactions are shown by green circles in all 2-dimensional figures.
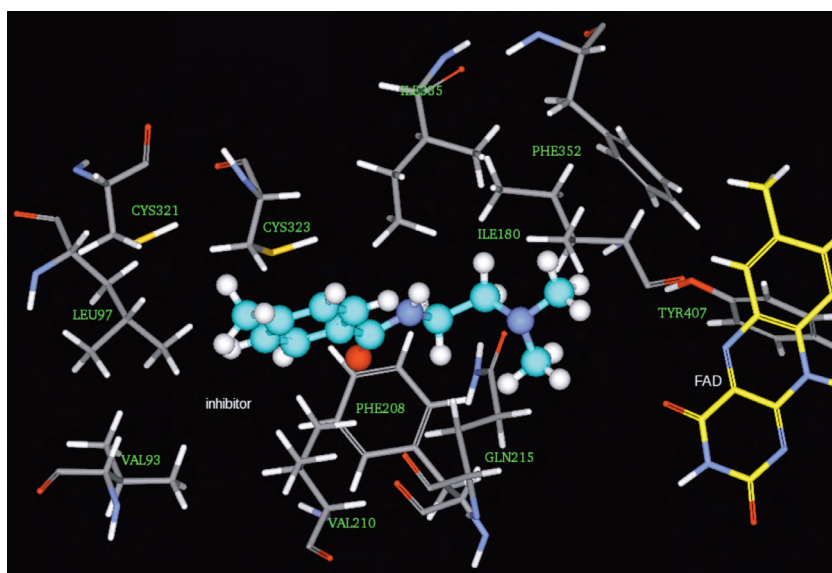
Figure 5. The 3-dimensional orientation of compound **2** in the active site of the MAO-A enzyme (see caption of Figure 3).
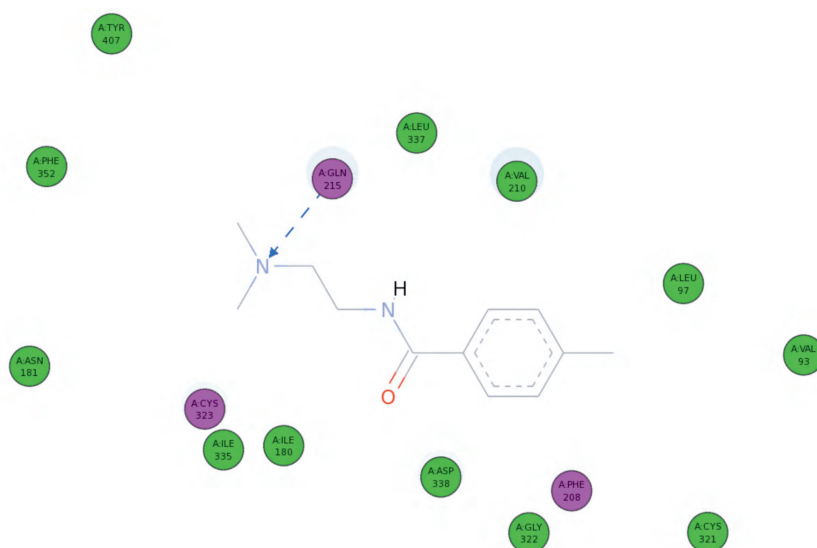

Figure 6. The 2-dimensional picture of compound **2** in the active site of the MAO-A enzyme (see caption of Figure 4).
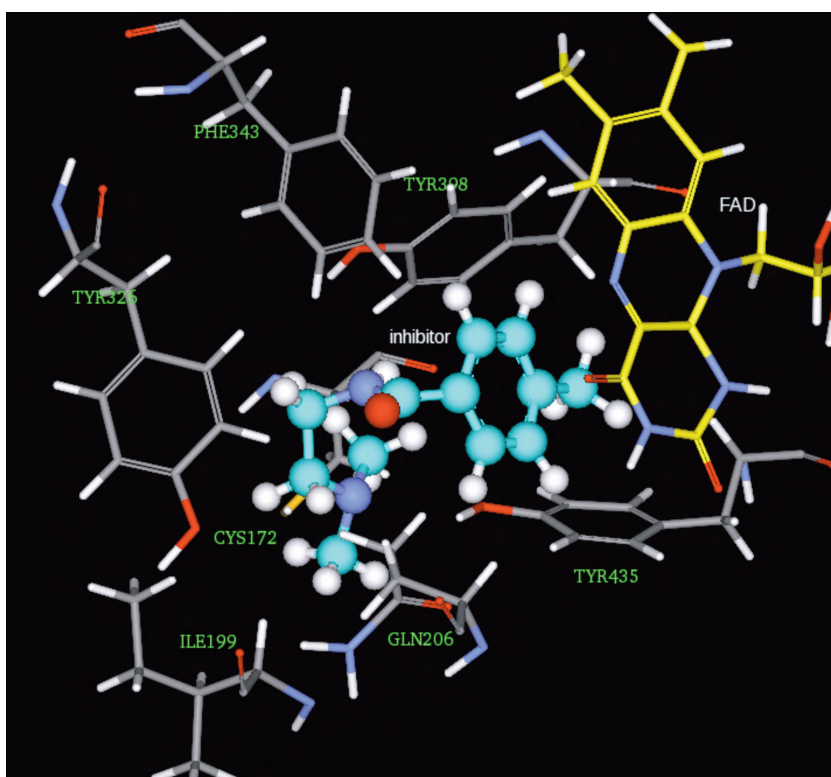
Figure 7. The 3-dimensional orientation of compound **2** in the active site of the MAO-B enzyme (see caption of Figure 3).
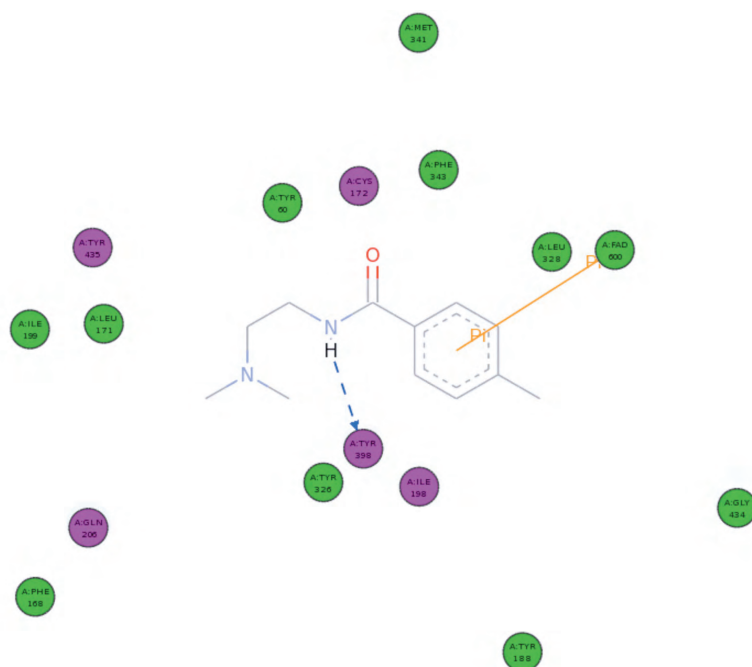

Figure 8. The 2-dimensional picture of compound **2** in the active site of the MAO-B enzyme (see caption of Figure 4).

Figures 7 and 8 show the best pose of compound **2** in the active site of MAO-B. From the 2D picture, 11 vdW interactions between the inhibitor and MAO-B can be detected. There is only one hydrogen bond between the amide hydrogen of the inhibitor and TYR398. The other contributing polar residues are CYS172, TYR435, and GLN206. However, the average distance between the receptor and inhibitor was higher than the value obtained for LSD1 and MAO-A. In addition, the positive value of the scoring energy, which is +61.58 kcal/mol, shows that the binding mode is not as favorable as in LSD1 and MAO-A.

The 3- and 2-dimensional pictures of the best pose of compound **5** in LSD1 are shown in Figures 9 and 10, respectively. There are 17 vdW interactions in the vicinity of 3.5 Å in the active site of LSD1. Compound **5** binds to LSD1 with almost the same strength as compound **2,** with a scoring energy of –21.68 kcal/mol. The FAD cofactor of the enzyme is at a close distance to the N-methyl tail of compound **5**, making one polar interaction. Another polar interaction is between CYS360 and the methoxy group of compound **5**.
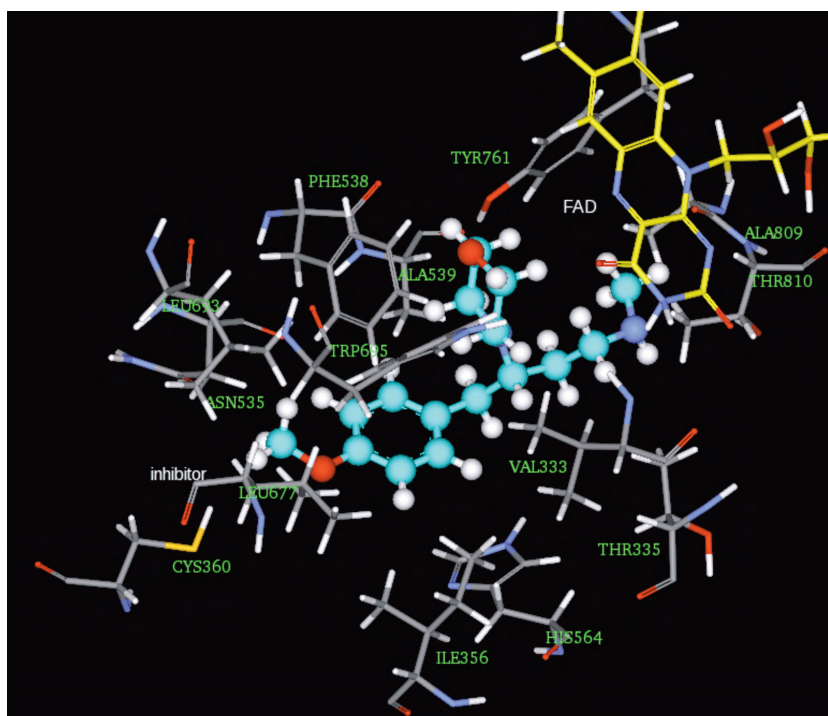

Figure 9. The 3-dimensional orientation of compound **5** in the active site of the LSD1 enzyme (see caption of Figure 3).

The best pose of compound **5** in the active site of the MAO-A enzyme is shown in Figures 11 and 12. From the 2D picture, 14 vdW interactions, 1 polar interaction between GLN215 and the morpholine nitrogen of compound **5**, and 1 $\pi - \sigma$ interaction between the methoxy group of the inhibitor and the FAD cofactor can be observed. Due to greater distances between the receptor and inhibitor, the binding affinity was not as strong as in LSD1, generating a positive CDOCKER energy value of +67.0 kcal/mol.

Finally, the best poses of compound **5** in the active site of MAO-B are shown in Figures 13 and 14, where one can detect 12 vdW attractions and 2 polar attractions between the FAD cofactor and the N-methyl amine group of the inhibitor and TYR188 and the methoxy group of the inhibitor. Additionally, there is one $\pi - \pi$

interaction between the phenyl ring of the inhibitor and the TYR435 side chain. However, similar to MAO-A, the average distance between the inhibitor and protein was relatively higher than in LSD1, resulting in a highly positive CDOCKER energy value of +248.9 kcal/mol. The 3-dimensional orientation of compound **5** in the active site of the LSD1 enzyme is also shown in Figure 15.
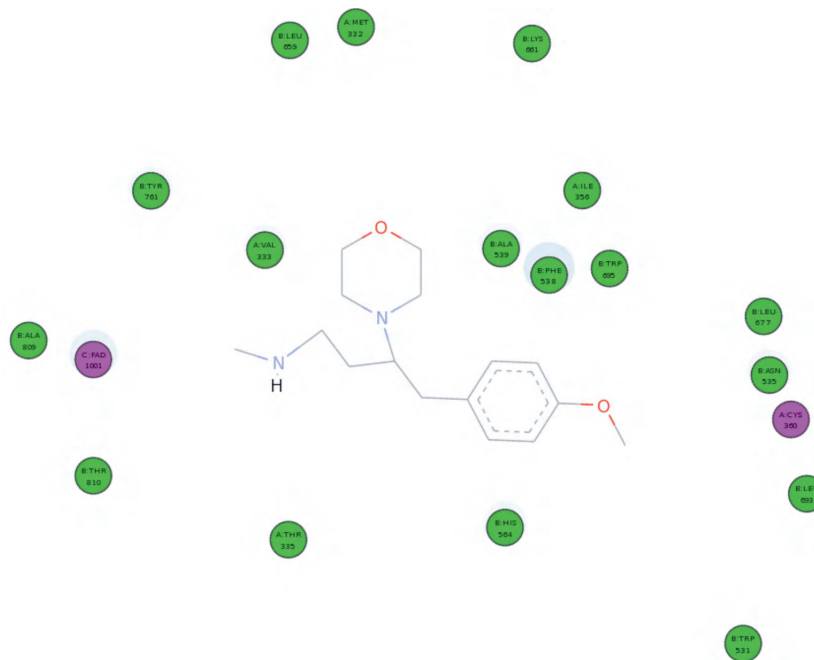

Figure 10. The 2-dimensional picture of compound **5** in the active site of the LSD1 enzyme (see caption of Figure 4).
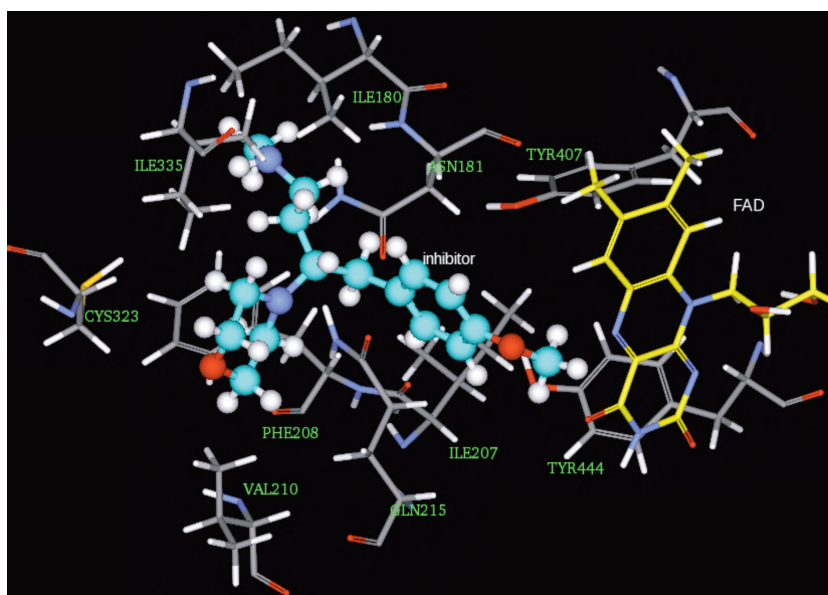

Figure 11. The 3-dimensional orientation of compound **5** in the active site of the MAO-A enzyme (see caption of Figure 3).
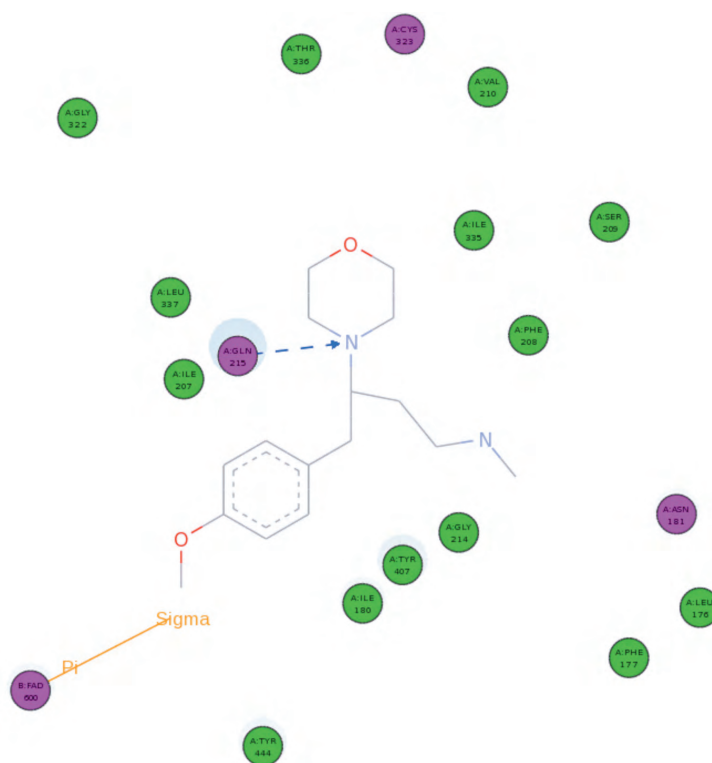
Figure 12. The 2-dimensional picture of compound **5** in the active site of the MAO-A enzyme (see caption of Figure 4).
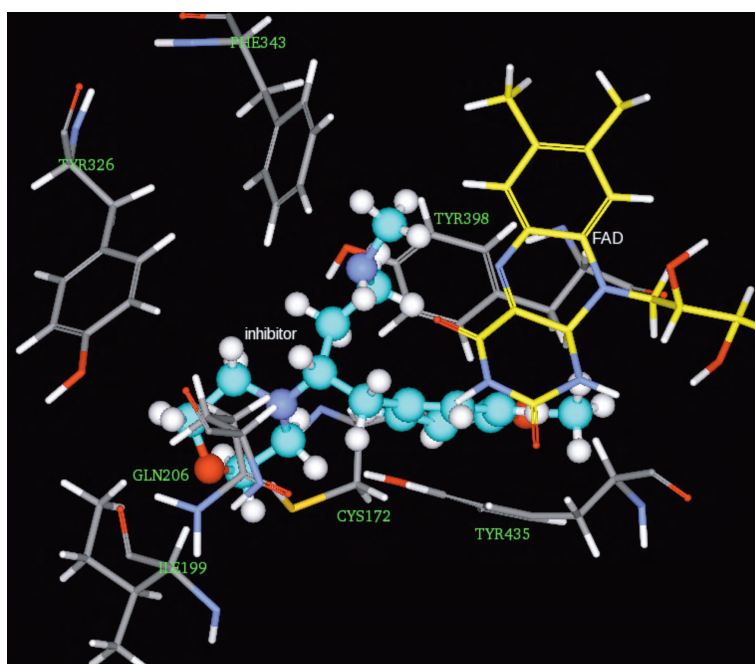

Figure 13. The 3-dimensional orientation of compound **5** in the active site of the MAO-B enzyme (see caption of Figure 3).
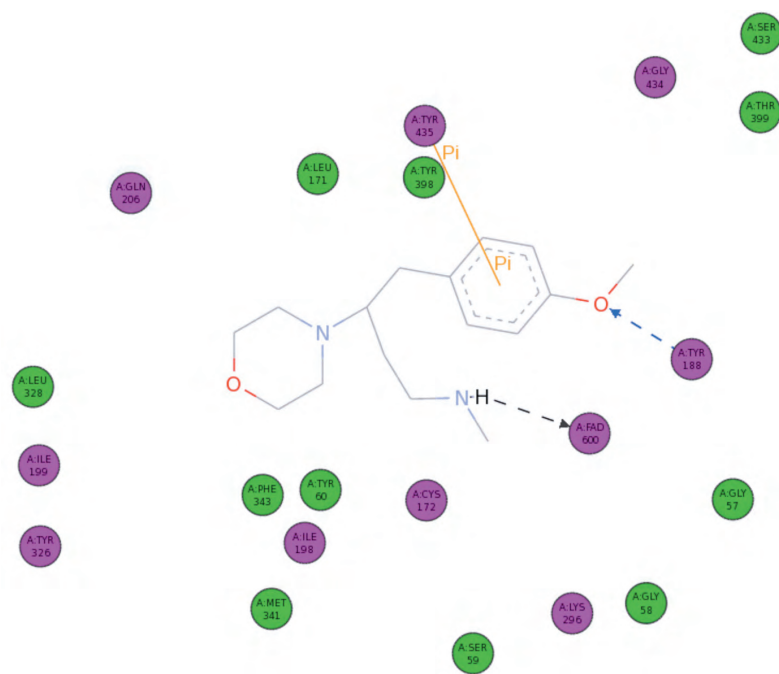
Figure 14. The 2-dimensional picture of compound **5** in the active site of the MAO-B enzyme (see caption of Figure 4).
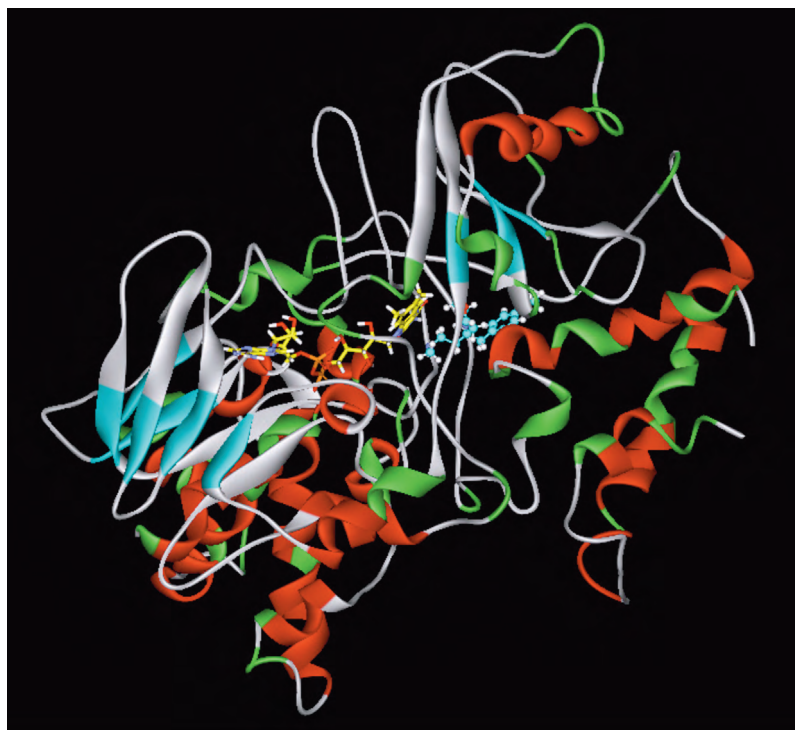

Figure 15. The 3-dimensional orientation of compound **5** in the active site of the LSD1 enzyme. Enzyme is shown as a flat ribbon, inhibitor is shown as a ball and stick, and cofactor FAD is depicted as yellow sticks on the left side of the inhibitor.

Conclusion

Computational results clearly show that tranylcypromine enantiomers selectively inhibit MAO-B with respect to LSD1 and MAO-A enzymes, in good agreement with the reported experimental results. Our current design and computational evaluation of 10 potential LSD1 selective inhibitors using various docking tools resulted in an almost 3-fold improvement of inhibitory activity with respect to tranylcypromine enantiomers and 2-[4-methoxy-phenyl]cyclopropylamine. Small differences in the conformations of the 3 proteins around their FAD regions, as discussed above, were the determining factors for the selectivity of the compounds for the respective proteins. In addition, the compounds showed excellent ADMET properties. Computer-aided drug design of our novel drug candidates for lysine-specific demethylase enzyme (LSD1), reported in this present study, will be a starting point for searching for new chromatin modifiers.

Acknowledgements

References

1. Shi, Y. J.; Lan, F.; Matson, C.; Mulligan, P.; Whetstine, J. R.; Cole, P. A.; Casero, R. A.; Shi, Y. *Cell* **2004**, *119*, 941-953.

2. Metzger, E.; Wissmann, M.; Yin, N.; Muller, J. M.; Schneider, R.; Peters, A.; Gunther, T.; Buettner, R.; Schule, R. *Nature* **2005**, *437*, 436-439.

3. You, A.; Tong, J. K.; Grozinger, C. M.; Schreiber, S. L. *PNAS* **2001**, *98*, 1454-1458.

4. Wang, G. G.; Allis, C. D.; Chi, P. *Trends Mol. Med.* **2007**, *13*, 363-372.

5. Kahl, P.; Gullotti, L.; Heukamp, L. C.; Wolf, S.; Friedrichs, N.; Vorreuther, R.; Solleder, G.; Bastian, P. J.; Ellinger, J.; Metzger, E.; Schule, R.; Buettner, R. *Cancer Res.* **2006**, *66*, 11341-11347.

6. Schmidt, D. M. Z.; McCafferty, D. G. *Biochemistry* **2007**, *46*, 4408-4416.

7. Huang, Y.; Greene, E.; Stewart, T. M.; Goodwin, A. C.; Baylin, S. B.; Wostert, P. M.; Casero, R. A. *PNAS* **2007**, *104*, 8023-8028.

8. Tsukada, Y.; Fang, J.; Erdjument-Bromage, H.; Warren, M. E.; Borchers, C. H.; Tempst, P.; Zhang, Y. *Nature* **2006**, *439*, 811-816.

9. Whetstine, J. R.; Nottke, A.; Lan, F.; Huarte, M.; Smolikov, S.; Chen, Z. Z.; Spooner, E.; Li, E.; Zhang, G. Y.; Colaiacovo, M.; Shi, Y. *Cell* **2006**, *125*, 467-481.

10. Chen, Z. Z.; Zang, J. Y.; Whetstine, J.; Hong, X.; Davrazou, F.; Kutateladze, T. G.; Simpson, M.; Mao, Q. L.; Pan, C. H.; Dai, S. D.; Hagman, J.; Hansen, K.; Shi, Y.; Zhang, G. Y. *Cell* **2006**, *125*, 691-702.

11. Xiang, Y.; Zhu, Z. Q.; Han, G.; Lin, H. Q.; Xu, L. Y.; Chen, C. D. *Cell Res.* **2007**, *17*, 850-857.

12. Rose, N. R.; Woon, E. C. Y.; Kingham, G. L.; King, O. N. F.; Mecinovic, J.; Clifton, I. J.; Ng, S. S.; Talib-Hardy, J.; Oppermann, U.; McDonough, M. A.; Schofield, C. J. *J. Med. Chem.* **2010**, *53*, 1810-1818.

13. Balciunas, D.; Ronne, H. *Trends Biochem. Sci.* **2000**, *25*, 274-276.

14. Erdem, S. S.; Karahan, Ö.; Yıdız, İ.; Yelekçi, K. *Org. Biomol. Chem.* **2006**, *4*, 646-658.

15. Yelekçi, K.; Karahan, Ö.; Toprakçı, M. *J. Neural Transm.* **2007**, *114*, 725-732.

16. Mimasu, S.; Sengoku, T.; Fukuzawa, S.; Umehara, T.; Yokoyama, S. *Biochem. Bioph. Res. Co.* **2008**, *366*, 15-22.

17. Chen, Y.; Yang, Y. T.; Wang, F.; Wan, K.; Yarnane, K.; Zhang, Y.; Lei, M. *PNAS* **2006**, *103*, 13956-13961.

18. Fraaije, M. W.; van Berkel, W. J. H.; Benen, J. A. E.; Visser, J.; Mattevi, A. *Trends Biochem. Sci.* **1998**, *23*, 206-207.

19. Fraaije, M. W.; Mattevi, A. *Trends Biochem. Sci.* **2000**, *25*, 126-132.

20. Forneris, F.; Binda, C.; Adamo, A.; Battaglioli, E.; Mattevi, A. *J. Biol. Chem.* **2007**, *282*, 20070-20074.

21. Wolber, G.; Langer, T. In *13th European Symposium on Quantitative Structure-Activity Relationships*; Prous Science, Dusseldorf, Germany, 2000.

22. Wu, G. S.; Robertson, D. H.; Brooks, C. L.; Vieth, M. *J. Comput. Chem.* **2003**, *24*, 1549-1562.

23. Jones, G.; Willett, P.; Glen, R. C. *J. Mol. Biol.* **1995**, *245*, 43-53.

24. Morris, G. M.; Goodsell, D. S.; Halliday, R. S.; Huey, R.; Hart, W. E.; Belew, R. K.; Olson, A. J. *J. Comput. Chem.* **1998**, *19*, 1639-1662.

25. Brooks, B. R.; Bruccoleri, R. E.; Olafson, B. D.; States, D. J.; Swaminathan, S.; Karplus, M. *J. Comput. Chem.* **1983**, *4*, 187-217.

26. Vieth, M.; Hirst, J. D.; Kolinski, A.; Brooks, C. L. *J. Comput. Chem.* **1998**, *19*, 1612-1622.

27. Shoichet, B. K.; Kuntz, I. D. *J. Mol. Bio.* **1991**, *221*, 327-346.

28. Walls, P. H.; Sternberg, M. J. E. *J. Mol. Bio.* **1992**, *228*, 277-297.

29. Miranker, A.; Karplus, M. *Proteins* **1991**, *11*, 29-34.

30. Jain, A. K.; Dubes, R. C. *Algorithms for Clustering Data*, Prentice Hall, Englewood Cliffs, NJ, 1988.

31. Weiner, P. K.; Kollman, P. A. *J. Comput. Chem.* **1981**, *2*, 287-303.

32. Weiner, S. J.; Kollman, P. A.; Case, D. A.; Singh, U. C.; Ghio, C.; Alagona, G.; Profeta, S.; Weiner, P. *J. Am. Chem. Soc.* **1984**, *106*, 765-784.

33. Weiner, S. J.; Kollman, P. A.; Nguyen, D. T.; Case, D. A. *J. Comput. Chem.* **1986**, *7*, 230-252.

34. Huey, R.; Morris, G. M.; Olson, A. J.; Goodsell, D. S. *J. Comput. Chem.* **2007**, *28*, 1145-1152.

35. Yang, M. J.; Culhane, J. C.; Szewczuk, L. M.; Jalili, P.; Ball, H. L.; Machius, M.; Cole, P. A.; Yu, H. T. *Biochemistry* **2007**, *46*, 8058-8065.

36. Binda, C.; Valente, S.; Romanenghi, M.; Pilotto, S.; Cirilli, R.; Karytinos, A.; Ciossani, G.; Botrugno, O. A.; Forneris, F.; Tardugno, M.; Edmondson, D. E.; Minucci, S.; Mattevi, A.; Mai, A. *J. Am. Chem. Soc.* **2010**, *132*, 6827-6833.